Real Aperture Imaging using Sparse Optimisation with Application to Low-Angle Tracking

Paul E. Berry and Sandun Kodituwakku
Defence Science and Technology Group, Edinburgh SA 5111, Australia.
Email: paul.berry@dst.defence.gov.au

***Abstract*—Estimating the angle of arrival of a low-altitude target over the sea surface is made difficult due to the coherent multipath interference caused by the target image. A real aperture imaging technique for estimating azimuth and elevation of targets using a phased array multichannel radar, as described by Berry *et al* [1], is applied to this classical problem of suppressing low-angle multipath signals received by a naval radar from a low-flying target. The degree of spatial resolution which can be usefully attained is explored; this depends on many factors and the nonlinear problem formulation is not easily amenable to analysis. It is found that the technique is feasible for resolving the direct target signal, its specular reflection and multiple diffuse reflections even when the signals would be combined by a conventional beamformer to form a multipath null.**

Keywords*—radar signal processing, multipath propagation, phased array multichannel radar, sparse optimisation, low-angle tracking.

I. Introduction

The low-angle tracking problem has its genesis in the difficulties encountered in tracking targets flying at sufficiently low altitudes above the sea surface that they are within a beamwidth of the horizon. The multipath returns thus created by reflections from the surface combine destructively at particular ranges to produce multipath propagation nulls, resulting in missed detections which impact upon the performance of the tracker. Furthermore, even at ranges where destructive superposition does not occur and a target is detected, its angular estimation using monopulse methods is deleteriously affected by the presence of multipaths, which expect a single dominant scatterer to reside within a range-Doppler cell. The problem of multipath nulls can be overcome by a simple change in operating frequency which effectively displaces the propagation null in range, but this does not address the angle estimation problem which seeks to estimate target direction to within $1/100$ th of a beamwidth.

The multipath rays comprise a coherent specular component with deterministic phase and multiple diffuse components caused by reflections from the glistening region with random phases (see Figure 1). In a smooth sea the specular multipath signal dominates the multipath returns and is virtually indistinguishable from the direct path signal, lying within the same range-Doppler cell and having a closely similar direction of arrival. In rough seas the diffuse multipath components tend to dominate over the specular return. The interference created by the multipaths has been a longstanding problem for shipboard radar systems (see Barton [2] for an early paper) and has been the subject of extensive investigation ([3]–[13]).

Approaches considered to address the problem include angular superresolution methods, such as MUSIC, but these require the signals to be uncorrelated, which the direct and specular mutipath signals are not. In some work, switching frequencies from pulse to pulse has been proposed as a way of decorrelating the signals. Maximum Likelihood and Maximum Entropy [14] techniques are able to resolve angular separations to high accuracy but depend upon numerical optimisation for practical implementation. Methods are also limited by the geometric assumptions underlying their inherent signal models and as a consequence may not be robust to all environmental conditions such as the effects of anomalous propagation. The flexibility of modern AESA radars provides the potential to fully exploit multichannel data and explore more general approaches which are less constrained by particular radar system architectures and signal modelling assumptions.

The approach adopted in this paper is less restrictive in terms of modelling assumptions, employing direct cross-aperture imaging using a sparse approximation problem formulation solved using an efficient nonlinear algorithm. The only assumptions inherent in this approach are that the array manifold is known (i.e. the phased array antenna has been suitably calibrated) and that the signals are *sparse* in the sense that the discrete directional target and interference signals are relatively small in number.

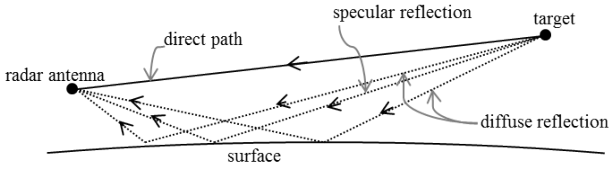

Fig. 1: Multipath propagation scenario.

The paper is organised as follows. A signal model is developed in Section II for the purpose of simulating the multipath signals received by a radar in a low-angle scenario. Section III formulates the inverse problem for the angle estimation and Section IV develops an algorithm for solving it. Section V provides results obtained using the angle estimation algorithm for the simulated signals. Finally, Section VI discusses the results obtained and proposes future work.

II. Multipath Surface Reflection Model

In order to demonstrate the performance of the proposed estimation algorithm it is necessary to simulate the multipath signals that would be received by a shipborne radar system under prevailing low-angle conditions. Suitable models have been developed over the years for this purpose beginning with Barton [2] and more recently [9], [10]. The geometry of multipath propagation is illustrated in Figure 2. The spherical earth geometry was used, and the target was assumed to be in the interference region where ray optic theory is valid. Here, the shipborne radar is positioned at R with antenna height h_r from the sea surface, and a low-altitude moving target is positioned at T with altitude h_t. The specular reflection point is denoted by S. The target image below the sea surface will be seen by the radar in this direction. Given h_r, h_t, and target range r_t, we compute all the other distances and angles required for signal modelling using this geometry.

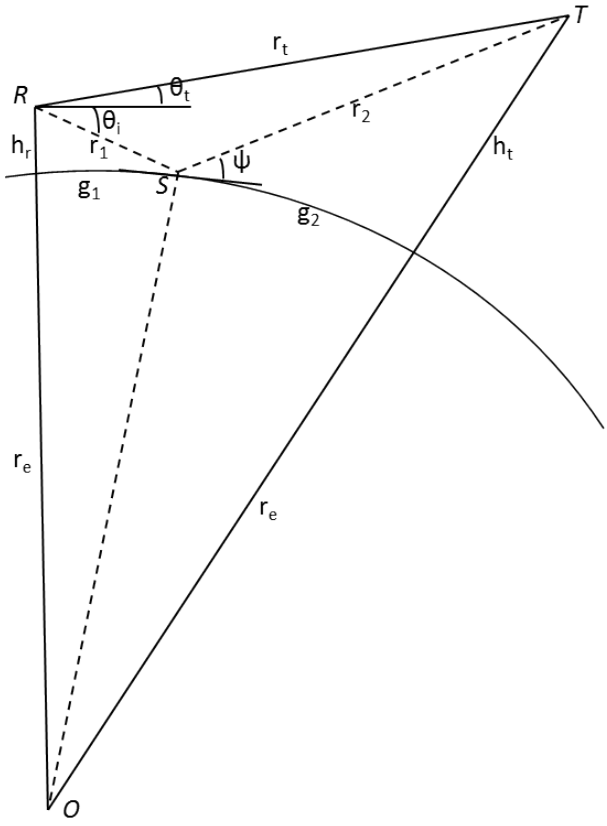

Fig. 2: Geometry of multipath propagation.

R = radar position
T = target position
O = effective centre of earth
S = specular reflection point
h_r = radar antenna height
h_t = target height
r_t = target range
r_1 = distance from radar to S
r_2 = distance from target to S
r_e = effective earth radius
g_1 = ground distance from radar to S
g_2 = ground distance from target to S
θ_t = target elevation angle
θ_i = image depression angle
ψ = grazing angle at the reflection point

Applying the cosine rule to ROT we obtain the target elevation angle

$$\theta_t = \sin^{-1}\left[\frac{(h_t + r_e)^2 - (h_r + r_e)^2 - r_t^2}{2(h_r + r_e)r_t}\right]. \quad (1)$$

The ground distance from the radar to the target $g = g_1 + g_2$. Applying the cosine rule to the same triangle, we get

$$g = 2r_e \sin^{-1}\left[\frac{r_t^2 - (h_t - h_r)^2}{4(h_r + r_e)(h_t + r_e)}\right]^{1/2}. \quad (2)$$

We can compute g_1 and g_2 as below.

$$g_1 = g/2 - p\sin(\xi/3) \quad (3)$$

where

$$p = \frac{2}{\sqrt{3}}\left[r_e(h_r + h_t) + (g/2)^2\right]^{1/2}, \quad (4)$$

and

$$\xi = \sin^{-1}\left[2r_e\, g(h_t - h_r)/p^3\right]. \quad (5)$$

Refer to Equations (2.50)–(2.52) in Skolnik's Radar handbook (2nd ed.) [15] for this calculation of g_1.

r_1 and r_2 can also be computed by the cosine rule to ROS and TOS respectively, as

$$r_1 = \left[(h_r + r_e)^2 + r_e^2 - 2(h_r + r_e)r_e\cos(g_1/r_e)\right]^{1/2} \quad (6)$$

and

$$r_2 = \left[(h_t + r_e)^2 + r_e^2 - 2(h_t + r_e)r_e\cos(g_2/r_e)\right]^{1/2}. \quad (7)$$

Then, the depression angle of the specular return θ_i and the grazing angle at the reflection point ψ can be computed as

$$\theta_i = \sin^{-1}\left[\frac{h_r^2 + r_1^2 + 2h_r r_e}{2(h_r + r_e)r_1}\right] \quad (8)$$

and

$$\psi = \sin^{-1}\left[\frac{h_r^2 - r_1^2 + 2h_r r_e}{2r_1 r_e}\right] \quad (9)$$

respectively.

The reflection coefficient is given by

$$\rho = \kappa D \rho_0. \quad (10)$$

The roughness factor κ accounts for the reduction in specular reflection coefficient due to the roughness of the reflection surface, and is given by [15]

$$\kappa = \exp\left[-2\left(\frac{2\pi H \sin\psi}{\lambda}\right)^2\right]. \quad (11)$$

For a sea surface which is considered here, H is the standard deviation of the wave height. H is approximately equal to $0.25H_{1/3}$, where significant wave height $H_{1/3}$ is defined as the average crest to trough height of the highest one-third of the waves. The divergence factor D accounts for the reduction in the specular reflection coefficient due to the earth's curvature, and is approximated by [15]

$$D = \left[1 + \frac{2g_1 g_2}{r_e g \sin\psi}\right]^{-1/2}. \tag{12}$$

The smooth flat-earth reflection coefficient is denoted by ρ_0, and is a function of the dielectric constant and the conductivity of the sea which can be empirically related to the sea temperature and salinity. The calculated values of ρ_0 for sea water of average salinity and temperature are given in Figures 2.12–2.14 of [15] for different grazing angles, polarisations, and frequencies, and used in our analysis.

The phase difference $\Delta\phi$ between the direct path and the specular reflection path consists of two components, one due to different lengths of two paths and the other due to phase change at the ground reflection, and can be written as

$$\Delta\phi = \frac{2\pi(r_1 + r_2 - r_t)}{\lambda} + \angle\rho_0. \tag{13}$$

In practical scenarios of interest, $\theta_t + \theta_i$ is a fraction of a beamwidth thus a conventional monopulse system fails to recover these multipaths, which would constructively or destructively interfere thereby degrading the radar track performance. The sparse representation and reconstruction algorithm presented in this paper has the potential to recover the multipaths, therefore maintaining good detection and tracking of low altitude targets.

III. Inverse Problem Formulation

A precursor to being able to estimate the angles of arrival is to specify the inverse problem which relates them to the measurements obtained. To this end, consider an $M \times N$-element Uniform Planar Array with element spacings d_x and d_y in the x and y-directions, boresight in the z-direction, wavelength λ, and azimuth angle ϕ and elevation θ to source. Then the Array Manifold is given by the set of steering vectors of length MN for all directions $0 \le \phi < 2\pi$ and $0 \le \theta \le \pi/2$, thus

$$\mathbf{s}(\theta,\phi) = \begin{pmatrix} 1 \\ \vdots \\ e^{2\pi j \frac{d_x}{\lambda}(m-1)\sin\theta\cos\phi} e^{2\pi j \frac{d_y}{\lambda}(n-1)\sin\theta\sin\phi} \\ \vdots \\ e^{2\pi j \frac{d_x}{\lambda}(M-1)\sin\theta\cos\phi} e^{2\pi j \frac{d_y}{\lambda}(N-1)\sin\theta\sin\phi} \end{pmatrix}.$$

Substituting $u_x = \sin\theta\cos\phi$ and $u_y = \sin\theta\sin\phi$, then $\sqrt{u_x^2 + u_y^2} = \sin^2\theta \le 1$ and

$$\mathbf{s}(u_x,u_y) = \mathbf{s}(u_x;d_x) \otimes \mathbf{s}(u_y;d_y) = \begin{pmatrix} 1 \\ \vdots \\ e^{2\pi j \frac{d_x}{\lambda}(m-1)u_x} e^{2\pi j \frac{d_y}{\lambda}(n-1)u_y} \\ \vdots \\ e^{2\pi j \frac{d_x}{\lambda}(M-1)u_x} e^{2\pi j \frac{d_y}{\lambda}(N-1)u_y} \end{pmatrix}.$$

We shall subsequently plot results in the unambiguous ψ_x, ψ_y-domain, where $\psi_x = \frac{2\pi d_x}{\lambda}\sin\theta\cos\phi$ and $\psi_y = \frac{2\pi d_y}{\lambda}\sin\theta\sin\phi$ with $\psi_x, \psi_y \in [-\pi, \pi]$.

We take $L > MN$ uniformly distributed spatial sampling points around the transmit direction in u_x, u_y - space to represent the array manifold and collect together their corresponding steering vectors to constitute the dictionary. These vectors compose the columns of the $MN \times L$ matrix S, which the observed signal $\mathbf{s}_0$ is represented in terms of, thus

$$\mathbf{s}_0 = \mathbf{S}\mathbf{a} \tag{14}$$

If the element spacings are a half wavelength or less then the Array Manifold mapping (in half-space) is one-to-one. However, if the element spacings are more than a half wavelength then the mapping is many-to-one which means that more than one direction can have the same array response such that the direction of origin of a given signal cannot be uniquely determined (the corresponding beampattern repetition in this instance is referred to as grating lobes).

It follows that the array response for a source with complex amplitude a at angles (θ, ϕ) is given by $a\mathbf{s}(\theta,\phi)$. In practice there will be additional interference in an observed set of array multichannel data $\mathbf{s}_0$ so the objective of a phase monopulse algorithm is to seek the best fit between the data and the signal model by, for instance, minimising the least-squares error, thus:

$$\min_{a,\theta,\phi}\{\|\mathbf{s}_0 - a\mathbf{s}(\theta,\phi)\|_2^2\}. \tag{15}$$

Least-squares approaches have the drawback of requiring prior knowledge of the number of sources. The following generalises the problem to the case of multiple scatterers where their number is unknown.

In accordance with the sparse approximation methodology, we propose that the observed signals can be represented as a sum of a relatively small number of discrete spatial source terms of the form $\mathbf{s}(\theta,\phi)$ residing within the main transmit beam which has direction (θ_{tx}, ϕ_{tx}). We take $L > MN$ uniformly-distributed spatial sampling points around the transmit direction (θ_{tx}, ϕ_{tx}) thus

$$\mathbf{s}_l = \mathbf{s}(\theta_l, \phi_l) \tag{16}$$

to represent the array manifold and collect together their corresponding array steering vectors to constitute the dictionary. These vectors, referred to in the sparse signal processing literature as *atoms*, compose the columns of the $MN \times L$

matrix $\mathbf{S}$ which the observed array response signal $\mathbf{b}$ is represented in terms of, thus

$$\mathbf{b} = \mathbf{S}\mathbf{a} + \mathbf{n} \tag{17}$$

where $\mathbf{n}$ is receiver noise. Because $L > MN$, this set of basis vectors is an over-complete representation for the received multichannel signal vector $\mathbf{b}$. We therefore seek the smallest number of non-vanishing complex coefficients a_l such that the observed signal $\mathbf{b}$, a single snapshot, can be expressed in terms of the dictionary $\{\mathbf{s}_l\}_{l=1}^{L}$, thus

$$\mathbf{b} = \mathbf{S}\mathbf{a}. \tag{18}$$

We could achieve this by solving the Basis Pursuit convex optimisation problem which uses the L_1 norm

$$\min_{\mathbf{a}}\{\|\mathbf{a}\|_1\} \tag{19}$$

subject to the constraint of equation (18). In practice, though, we need to account for the possibility of extraneous interference for which either no signal model is available or it is of unknown structure. In this instance the objective is to minimise the error between the observed signal and the model in the least-squares sense, while simultaneously attempting to minimise the number of non-vanishing coefficients, thus

$$\min_{\mathbf{a}}\{\|\mathbf{a}\|_1 + \mu\|\mathbf{S}\mathbf{a} - \mathbf{b}\|_2^2\} \tag{20}$$

for a suitable parameter $\mu > 0$. This problem formulation is known as Basis Pursuit Denoising.

IV. Solution Algorithm

A fast sparse functional iteration algorithm was proposed by the present authors in [1] and is summarised here. The problem formulation of (20) is an equality-constrained optimisation problem and is, in principle, solvable by the Lagrange Multiplier Method except for the fact that the l_1-norm is not differentiable at any point in the state space when any atom is zero. Since most of the atoms are expected to be zero in the solution which is sought, due to the assumption of sparsity, this is addressed by *smoothing* the l_1-norm; that is, replacing it with an approximate version which is differentiable as follows. The l_1-norm of $\mathbf{a}$ is the sum of the complex moduli of the components a_k of $\mathbf{a}$ thus

$$\|\mathbf{a}\|_1 = \sum_{l=1}^{L} |a_l| \tag{21}$$

which we may smooth by replacing the complex modulus $|a_l|$ by $\sqrt{|a_l|^2 + \delta}$ where δ is small, positive and non-zero. Hence

$$\|\mathbf{a}\|_1 \approx \sum_{l=1}^{L} \sqrt{|a_l|^2 + \delta} \tag{22}$$

The Lagrange multiplier method solves the optimisation problem by finding the stationary point of:

$$\sum_{l} \sqrt{|a_l|^2 + \delta} + \mu\|\boldsymbol{\epsilon}\|_2^2 + \mathbb{R}\{\boldsymbol{\lambda}^H\boldsymbol{\epsilon}\} \tag{23}$$

with respect to $\mathbf{a}$, $\boldsymbol{\epsilon}$ and $\boldsymbol{\lambda}$, and subject to

$$\mathbf{S}\mathbf{a} - \mathbf{b} = \boldsymbol{\epsilon} \tag{24}$$

where the complex vector $\boldsymbol{\lambda}$ comprises the Lagrange multipliers. At the stationary point the following nonlinear equations are satisfied which have been derived by complex differentiation and substitution,

$$\boldsymbol{\Lambda}^{-1}(\mathbf{a})\,\mathbf{a} + \mu\mathbf{S}^H(\mathbf{S}\mathbf{a} - \mathbf{b}) = 0 \tag{25}$$

where the $L \times L$ diagonal matrix

$$\boldsymbol{\Lambda}(\mathbf{a}) = \begin{bmatrix} \ddots & & \mathbf{0} \\ & g(a_l) & \\ \mathbf{0} & & \ddots \end{bmatrix} \tag{26}$$

with

$$g(a_l) = \sqrt{|a_l|^2 + \delta}. \tag{27}$$

We may rewrite the system in the form:

$$[\boldsymbol{I}_L + \mu\boldsymbol{\Lambda}(\mathbf{a})\mathbf{S}^H\mathbf{S}]\mathbf{a} = \mu\boldsymbol{\Lambda}(\mathbf{a})\mathbf{S}^H\mathbf{b} \tag{28}$$

and observe that this is a system of L nonlinear algebraic equations with unknown vector of complex amplitudes $\mathbf{a}$. This system could be solved using Newton-Raphson iteration but fortuitously it is amenable to solution by *functional iteration* which does not require computation of the Jacobian (see for example, [16] p85). Observing that the system can be written as

$$\mathbf{x} = \mathbf{f}(\mathbf{x}),$$

functional iteration proposes the solution algorithm

$$\mathbf{x}^{n+1} = \mathbf{f}(\mathbf{x}^n)$$

beginning with an initial guess $\mathbf{x}^0$.

The proposed Fast Sparse Functional Iteration Algorithm (FSFIA) is therefore:

$$[\boldsymbol{I}_L + \mu\boldsymbol{\Lambda}(\mathbf{a}^n)\mathbf{S}^H\mathbf{S}]\mathbf{a}^{n+1} = \mu\boldsymbol{\Lambda}(\mathbf{a}^n)\mathbf{S}^H\mathbf{b}. \tag{29}$$

Beginning with an initial guess (say) $a_i = 1\ \forall\ i$, the algorithm has been found to be both fast (converges in a few iterations to a good quality solution) and stable. Note that $\mathbf{S}^H\mathbf{b}$ is the set of correlations between data $\mathbf{b}$ and all of the atoms, as also required by greedy pursuit solution methods.

Most computational effort for the solution algorithm is involved in solving the linear system (29) at each iteration. This is an $L \times L$ system which, using Gaussian elimination, requires $O(L^3)$ floating-point operations where L is the number of atoms. Application of the Woodbury formula reduces the size to a generally much smaller $MN \times MN$ system, requiring only $O((MN)^3)$ floating-point operations per iteration.

V. Simulation Results

The multipath signal model of Section II is used to simulate the array signal response to the multipaths, and the sparse estimation algorithm of Section IV is used to estimate their angles of arrival. The direct and multipath returned signals estimated by the solution algorithm can be plotted in terms of their strengths in azimuth and elevation. The dictionary needs to be sufficiently dense to spatially resolve multipath signals which are in close proximity. Generally, a signal source will not coincide exactly in parameter space with an atom and so energy will spread to neighbouring atoms. The degree of spread will depend upon a number of factors such as the size of the dictionary, the number of channels, the antenna aperture, antenna calibration errors, the SNR and the number of iterations undertaken by FSFIA until convergence had been deemed to have been achieved.

It may be generally observed that when a dictionary is small (comprising relatively few, widely-spaced atoms in parameter space) then energy is spread into not only neighbouring atoms but beyond, and in low SNR situations spurious atoms occur unrelated to any true scatterers. However, a dense dictionary (many closely-spaced atoms in parameter space) is more robust, presumably because the scatterers are more accurately represented by atoms in their vicinity, and is particularly so at low SNR, though at additional computational cost. However, a dictionary which is too dense results in energy being spread due to coherence between atoms [17].

For a given range cell the elevation of the sea surface is known so any signals above that will correspond to targets of interest, whereas signals with below-surface elevations will correspond to multipaths. In the case of a smooth sea the strongest multipath signals will be images of the targets with phases shifted as a consequence of the path length differences and complex reflection coefficients. In the following analysis, we specify d_x/λ and d_y/λ such that, except for the reflection coefficient and phase difference between the direct and multipath signals, the result is frequency-independent as it depends only upon the geometry.

As an example we consider a radar antenna height of 15m, a target altitude of 40m above the sea surface and a range of 7.5km which, using the analysis of Section II, gives $\theta_t = 0.1657^\circ$ and $\theta_i = 0.4191^\circ$ at $\phi = 0^\circ$ and $\phi = \pi$ respectively. The antenna is a 25×25-element vertical array with element spacing 5λ and $SNR = 10dB$. The ψ_x, ψ_y domain is uniformly discretised into a 100×100 grid of atoms comprising the dictionary. This gives better control over the coherence of the atoms but results in nonuniformly distributed atoms in the θ, ϕ-domain.

It is seen in Figures 3 and 4 that in this case the algorithm successfully resolves the spatial signals by promoting the two nearest atoms to each of the multipaths. Here, the true scatterers are represented by diamond symbols, and are generally not aligned with the grid of atoms, whereas the estimated atom amplitudes are represented by discs and are aligned with a grid.

Figure 5 shows the result of decreasing the element spacing to $\lambda/2$ but with the same dictionary. The scatterers move together in the ψ_x-ψ_y domain to the point where the grid is

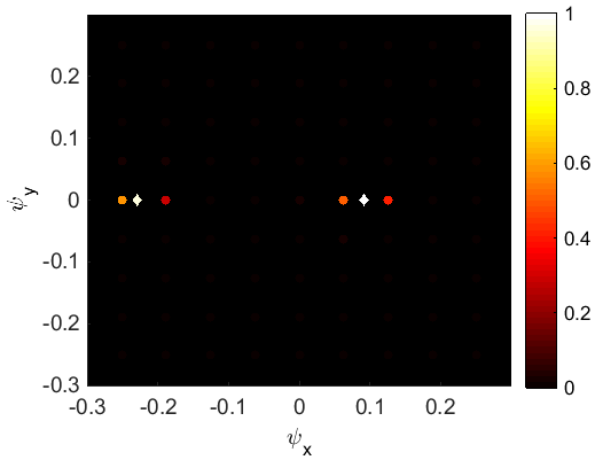

Fig. 3: Scatterers and atom intensities in ψ_x-ψ_y domain for $d = 5\lambda$

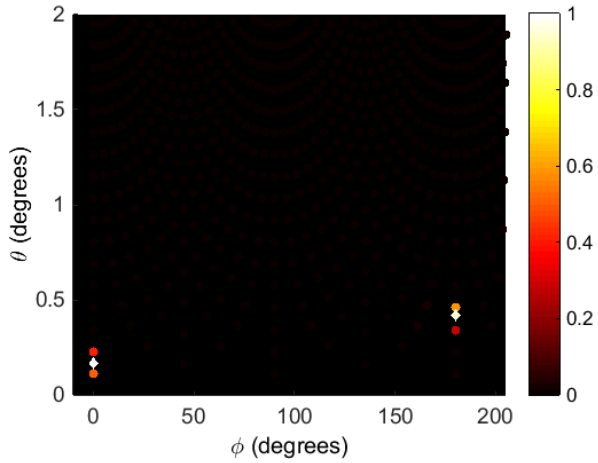

Fig. 4: Scatterers and atom intensities in θ-ϕ domain for $d = 5\lambda$

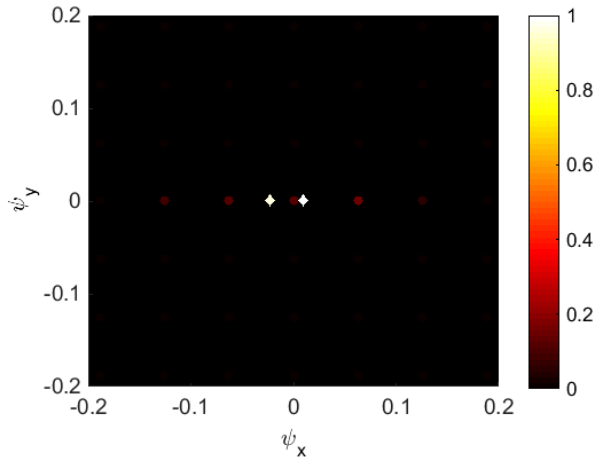

Fig. 5: Scatterers and atom intensities with element spacing of $\lambda/2$

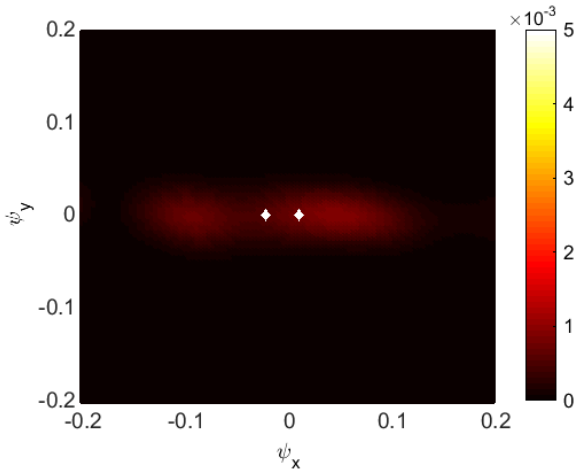

Fig. 6: Scatterers and atom intensities with element spacing of $\lambda/2$ and a denser grid

unable to resolve them. Figure 6 shows the result of attempting to refine the grid further locally so as to resolve the scatterers but energy is simply smeared locally across many atoms. This is a result of the fundamental problem of atom coherence in compressive spectral estimation discussed below.

VI. Discussion

It has been demonstrated that cross-range imaging using sparse approximation has the potential to spatially separate direct and multipath signals in a low-elevation target scenario. When modelled in the ψ_x, ψ_y-plane this is a classical spectral estimation problem with scatterers moving together in parameter space as element spacing decreases, and therefore becoming harder to distinguish. Increasing the density of atoms to enhance resolution, however, simply results in energy becoming smeared in the scatterers' vicinity which appears to fundamentally limit the achievable resolution. This may be explained by the atoms becoming increasingly coherent with their neighbours as their density in parameter space increases (see, for example, Duarte & Baraniuk [17]) and is a fundamental problem in compressive spectral estimation, requiring further investigation in the current context so as to achieve the desired angular resolution with reasonable aperture size. Further work is also required to explore the optimal design in terms of number of channels, size of dictionary, phase centre separation for azimuth and elevation, and robustness to noise.

VII. Conclusions

Direct cross-range imaging of a low-flying target in a low-elevation multipath scenario would enable the target to be spatially separated from any interference caused by specular and diffuse multipaths. This paper has shown that a spatial sparse approximation problem formulation coupled with a fast l_1 optimisation algorithm is able, in principle, to achieve the necessary resolution but not under all conditions likely to be met in practice. As it is independent of any geometrical modelling assumptions, it can be expected to be robust to varying environmental conditions which might break such assumptions inherent to other methods. Further work needs to be undertaken to resolve the problem of atom coherency which limits the achievable spatial resolution.

References

[1] P. E. Berry, S. Kodituwakku, and K. Venkataraman, "Generalised phase monopulse for multi-target DoA estimation and extended target spatial imaging," in *International Conference on Radar Systems (Radar 2017)*. IET, 2017.

[2] D. K. Barton, "Low-angle radar tracking," *Proceedings of the IEEE*, vol. 62, no. 6, pp. 687–704, 1974.

[3] A. Mrstik and P. Smith, "Multipath limitations on low-angle radar tracking," *IEEE transactions on aerospace and electronic systems*, no. 1, pp. 85–102, 1978.

[4] S. Haykin and J. Reilly, "Maximum-likelihood receiver for low-angle tracking radar. part 1: The symmetric case," in *IEE Proceedings F (Communications, Radar and Signal Processing)*, vol. 129, no. 4. IET, 1982, pp. 261–272.

[5] J. Reilly and S. Haykin, "Maximum-likelihood receiver for low-angle tracking radar. part 2: The nonsymmetric case," in *IEE Proceedings F (Communications, Radar and Signal Processing)*, vol. 129, no. 5. IET, 1982, pp. 331–340.

[6] M. D. Zoltowski and T.-S. Lee, "Maximum likelihood based sensor array signal processing in the beamspace domain for low angle radar tracking," *IEEE Transactions on signal processing*, vol. 39, no. 3, pp. 656–671, 1991.

[7] E. Bosse, R. Turner, and M. Lecours, "Tracking swerling fluctuating targets at low altitude over the sea," *IEEE Transactions on Aerospace and Electronic Systems*, vol. 27, no. 5, pp. 806–822, 1991.

[8] K.-B. Yu, "Recursive super-resolution algorithm for low-elevation target angle tracking in multipath," *IEE Proceedings-Radar, Sonar and Navigation*, vol. 141, no. 4, pp. 223–229, 1994.

[9] M. Sebt, A. Sheikhi, and M. Nayebi, "Robust low-angle estimation by an array radar," *IET radar, sonar & navigation*, vol. 4, no. 6, pp. 780–790, 2010.

[10] D. Park, E. Yang, S. Ahn, and J. Chun, "Adaptive beamforming for low-angle target tracking under multipath interference," *IEEE Transactions on Aerospace and Electronic Systems*, vol. 50, no. 4, pp. 2564–2577, 2014.

[11] Y. Cao, S. Wang, Y. Wang, and S. Zhou, "Target detection for low angle radar based on multi-frequency order-statistics," *Journal of Systems Engineering and Electronics*, vol. 26, no. 2, pp. 267–273, 2015.

[12] Y. Zheng, B. Chen, and M. Yang, "Cramer-rao bound of the estimation of direction of arrival for low angle targets," in *CIE International Conference on Radar*. IEEE, 2016, pp. 1–4.

[13] P. E. Berry and D. P. Finch, "Low-angle target detection with interference in a multipath environment," in *International Conference on Radar*. IEEE, 2013, pp. 440–445.

[14] W. White, "Low-angle radar tracking in the presence of multipath," *IEEE Transactions on Aerospace and Electronic Systems*, no. 6, pp. 835–852, 1974.

[15] M. I. Skolnik, *Radar handbook - 2nd ed.* McGraw-Hill Publishing, 1990.

[16] H. B. Keller and E. Isaacson, "Analysis of numerical methods," *New York*, 1966.

[17] M. F. Duarte and R. G. Baraniuk, "Spectral compressive sensing," *Applied and Computational Harmonic Analysis*, vol. 35, no. 1, pp. 111–129, 2013.